

# Structural analysis across length scales of the scorpion pincer cuticle

Israel Kellersztein<sup>a,1\*</sup>, Israel Greenfeld<sup>a,1</sup> and H. Daniel Wagner<sup>a,\*</sup>

<sup>a</sup>Department of Materials and Interfaces, Weizmann Institute of Science, Rehovot, 76100, Israel.

<sup>1</sup>These authors contributed equally to this work

\*Corresponding authors.

## Supporting Information

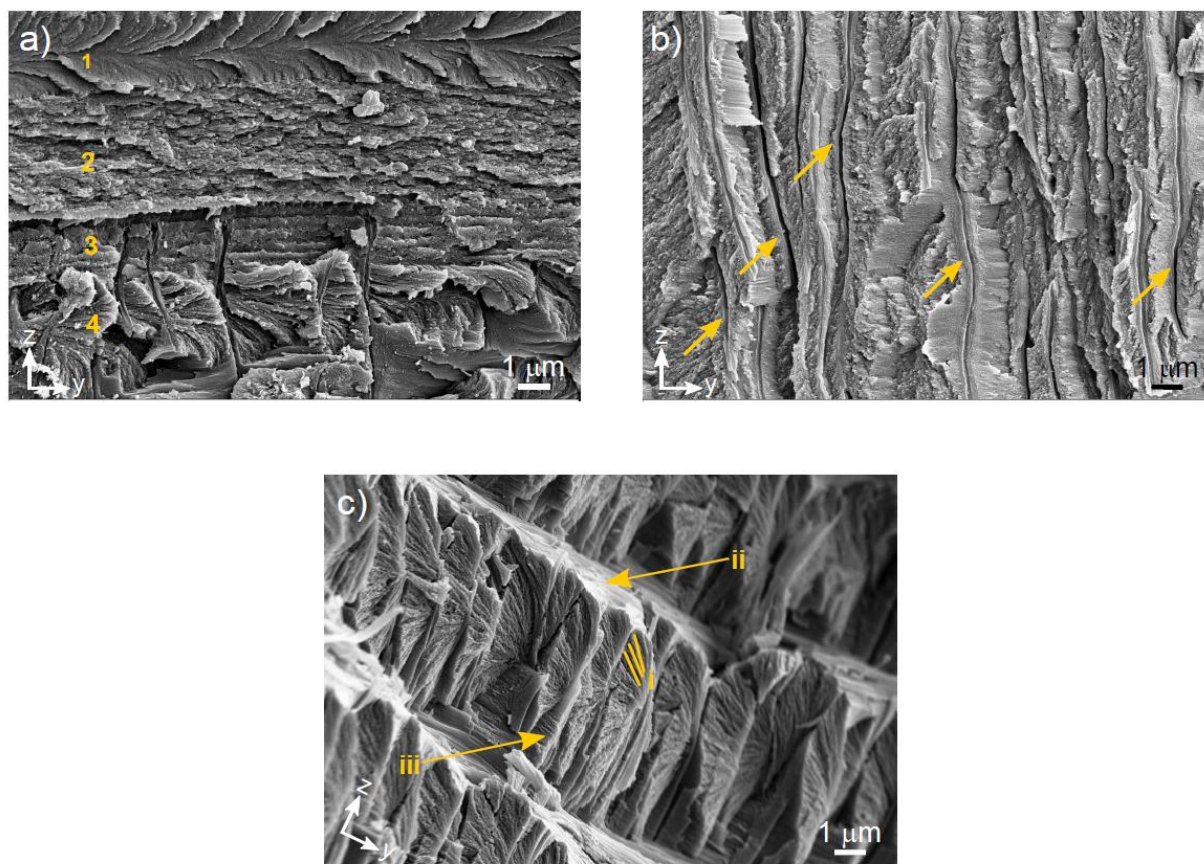


**Fig. S1 SEM transversal cross-section through the tibia layers.** **a)** The exocuticle is divided in four sublayers with different morphology (top-down): (1) a fibrous layer oriented to a certain orientation in relation to the  $x$ -axis, (2) an in-plane isotropic layer apparently made of a platelet-like structure, (3) a second fibrous layer oriented in the  $x$  direction, and (4) a layer of horizontally oriented layers composed of Bouligand units. **b)** The intermediate layer is apparently made of unidirectional discontinuous fibers closely oriented in the  $x$  direction and arranged in vertically oriented lamellae. The pore canals are pointed by yellow arrows. **c)** The endocuticle is made of horizontally oriented layers composed by Bouligand structural units. The SP cuticle Bouligand exhibits unique features [1], where (i) the different laminae are off-axis twisted and out-of-plane tilted, (ii) adjacent layers of Bouligands are separated by a interlayer whereas (iii) Bouligand units are separated by thinner intralayers.

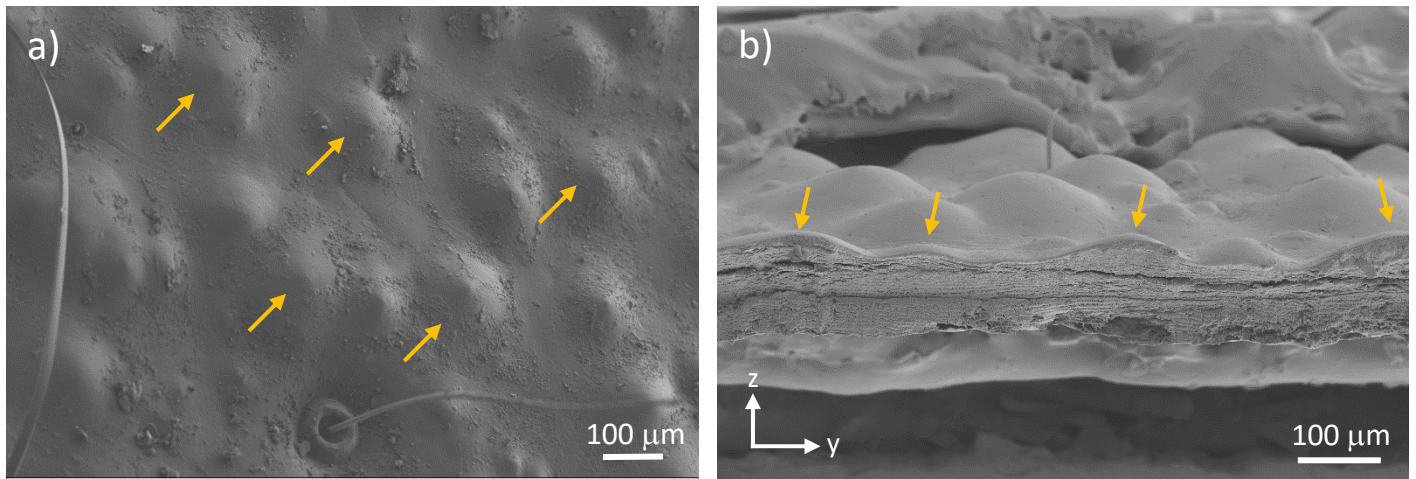


**Fig. S2 Topographical roughness of the tibia surface.** a) SEM image of a section in the SP tibia external surface displaying the “mountains” (pointed by yellow arrows); b) SEM image of a transversal (yz) cross-section of the tibia showing the thickness variance in the tissue due to the presence of such “mountains” (pointed by yellow arrows).

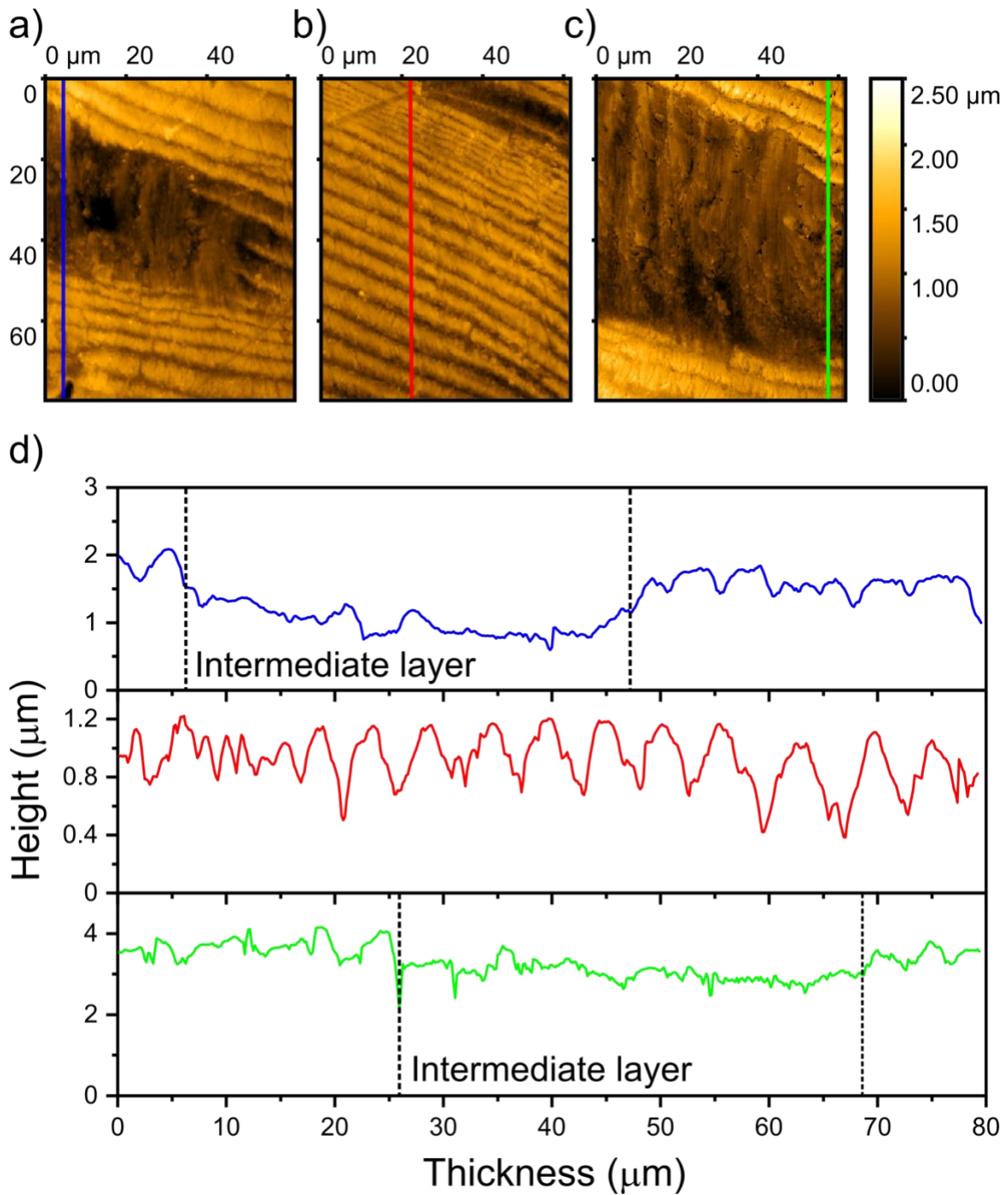


**Fig. S3 Full profiles from images shown in Fig. 2b-c in the main text.** The intermediate layer exhibits a thickness variance in the tibia exoskeleton, e.g. the intermediate layer in (a) is thinner than in (c), as seen by the profiles plot in (d). AFM image of (b) shows the lack of such intermediate layer.

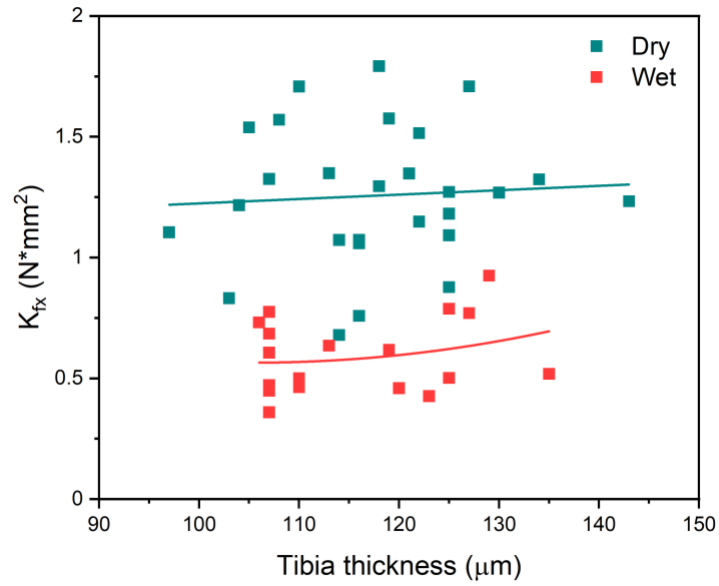


**Fig. S4 Bending stiffness of the tibia exoskeleton.** The bending stiffness increases as the tibia thickness grows, in contrast to the bending modulus which decreases as shown in Fig. 3c in the main text.

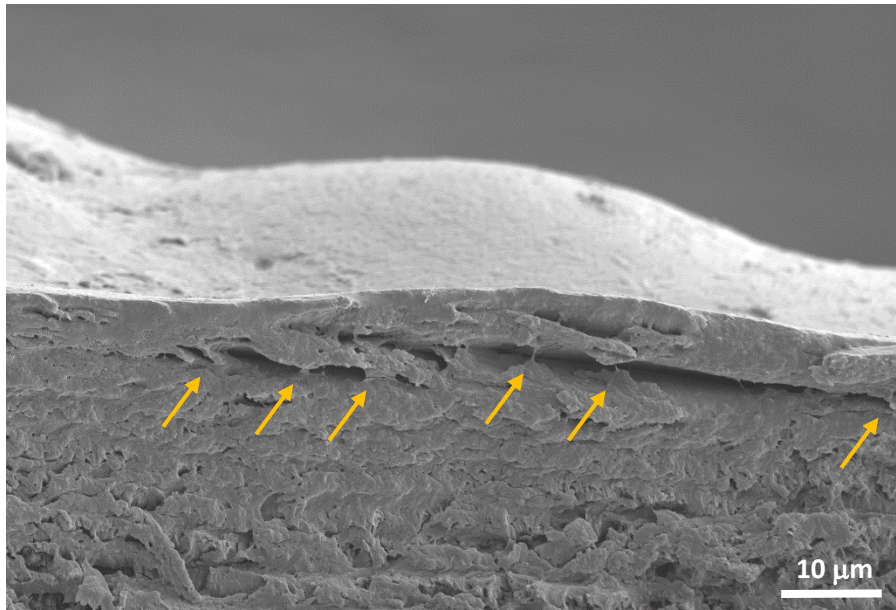


**Fig. S5 Fiber bridging in hydrated tibia samples.** Damage tolerance and diffused damage allow wet tibia samples to absorb a higher amount of energy, via toughening mechanisms such as fiber-matrix interface debonding and fiber bridging (pointed with yellow arrows).

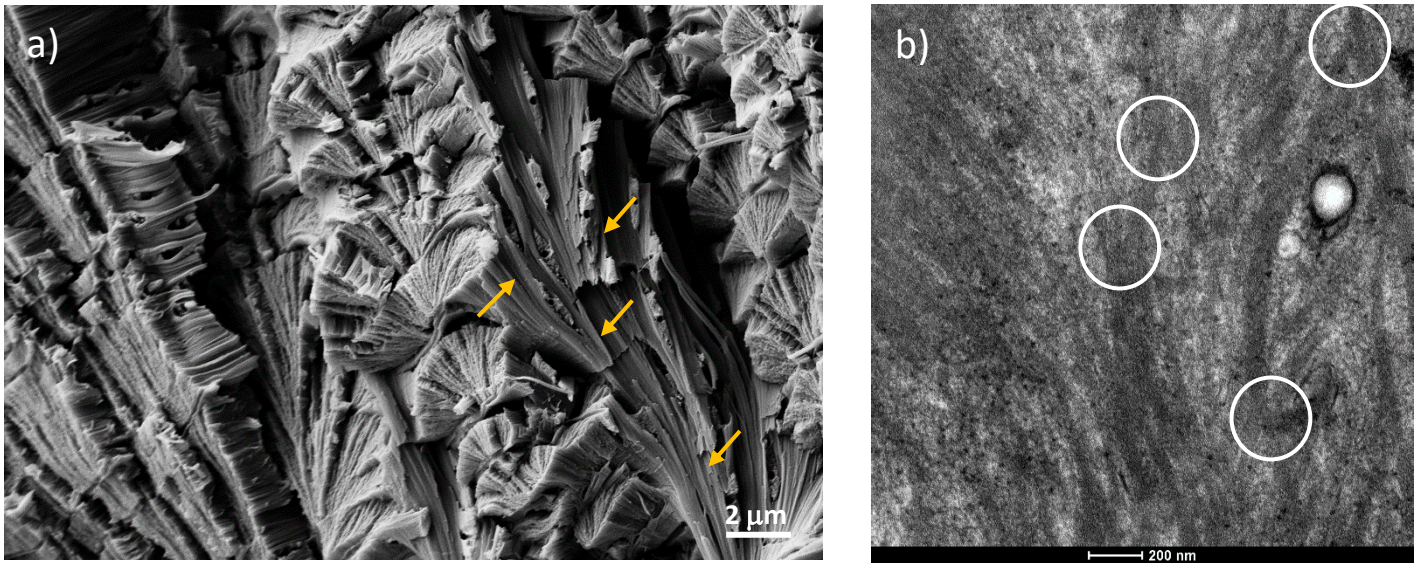


**Fig. S6 Shear interlocking and chitin fibers interconnections.** **a)** SEM image of an oblique view of the Bouligand arrangement within the endocuticle of the SP; the densely packed structure demonstrates the effect of shear interlocking between Bouligand units. **b)** TEM image of the interlayer in the endocuticle of the SP showing the chitin fibers (average diameter of 75 nm) and their interconnections (indicated by white circles); yellow arrows in **a)** display also such interconnections. The chitin-protein structure exposes a network-type architecture consisting of parallel and branched fibers; similar chitin interconnections were observed in the lobster exoskeleton [2]. Both shear interlocking and chitin fiber interconnections provide an additional mechanical stability of the cuticle by preventing displacement under shear and tensional stresses.

**Table S1:** Calculated elastic constants for lamina and Bouligands laminate unit (BLU)<sup>a</sup>.

Calculated lamina constants <sup>b,c</sup>			Calculated BLUs laminate constants <sup>c</sup>		
$E_1$	longitudinal modulus	35.0	$E_1$	longitudinal modulus	8.2
$E_2$	transversal modulus	2.6	$E_2$	transversal modulus	5.9
$G_{12}$	shear modulus	1.4	$G_{12}$	shear modulus	5.4
$\nu_{12}$	Poisson ratio	0.40	$\nu_{12}$	Poisson ratio	0.08
$\nu_{21}$	Poisson ratio	0.03	$\nu_{21}$	Poisson ratio	0.06

**Notes:**

- Units: elastic and flexural moduli are in GPa.
- Lamina and BLU constants adapted from [1], with adjustments for fiber and matrix properties, and incorporation of the shear interlocking and interconnecting effects.
- Lamina and BLUs elastic constants are in principal material axes (1,2), where the 1-axis co-aligns with the direction of the fibers in the lamina, in the case of BLU the midplane lamina.

**Table S2:** Calculated elastic constants for the exocuticle, intermediate layer, endocuticle and SP chela cuticle laminates<sup>a,b</sup>.

Exocuticle			Intermediate layer			Endocuticle			Cuticle laminate		
$E_x$	long. modulus	10.5	$E_x$	long. modulus	35.0	$E_x$	long. modulus	9.2	$E_x$	long. modulus	15.4
$E_y$	trans. modulus	10.4	$E_y$	trans. modulus	2.6	$E_y$	trans. modulus	8.8	$E_y$	trans. modulus	7.2
$G_{xy}$	shear modulus	3.3	$G_{xy}$	shear modulus	1.4	$G_{xy}$	shear modulus	4.1	$G_{xy}$	shear modulus	3.0
$\nu_{xy}$	Poisson ratio	0.12	$\nu_{xy}$	Poisson ratio	0.40	$\nu_{xy}$	Poisson ratio	0.09	$\nu_{xy}$	Poisson ratio	0.13
$\nu_{yx}$	Poisson ratio	0.18	$\nu_{yx}$	Poisson ratio	0.03	$\nu_{yx}$	Poisson ratio	0.08	$\nu_{yx}$	Poisson ratio	0.06
									$\bar{\eta}_{ij}$	shear coupling	0
									$E_{fx}$	bending modulus	11.7
									$E_{fy}$	bending modulus	8.5
									$E_S$	torsion modulus	3.3

**Notes:**

- a. Units: elastic and flexural moduli are in GPa.
- b. Laminate elastic constants are in principal laminate axis ( $x,y$ ).

**SI References:**

- [1] I. Greenfeld, I. Kellersztein, and H. D. Wagner, “Nested helicoids in biological microstructures,” *Nat. Commun.*, vol. 11, no. 224, 2020.
- [2] D. Raabe *et al.*, “Microstructure and crystallographic texture of the chitin–protein network in the biological composite material of the exoskeleton of the lobster *Homarus americanus*,” *Mater. Sci. Eng. A*, vol. 421, no. 1, pp. 143–153, 2006.